

Identification of Copper Surface Index by Optical Contrast

Zhibin Zhang, Xiaozhi Xu, Zhihong Zhang, Muhong Wu, Jinhuan Wang, Can Liu, Nianze Shang, Jinxiang Wang, Peng Gao, Dapeng Yu, Enge Wang, and Kaihui Liu*

With the rise of 2D materials, copper (Cu) is revealed as good surface catalyst, especially in the self-limited growth of graphene. In the regime of surface catalyst, the catalytic activities and functionalities of Cu should be highly dependent on its surface type. Traditional methods to determine the surface index are mainly high-vacuum based surface science techniques and are typically of low throughput and in small scale. A method to fast detect the surface index of Cu in large scale is still lacking. Here, the authors report an effective optical contrast method to identify the Cu surface index in large area. This method is based on the Cu₂O-thickness dependent color of Cu surface after a mild oxidation in hot air. It is revealed that different Cu surfaces (Cu(111), Cu(100), and Cu(110) as examples) have various oxidation barriers and would exhibit distinct color evolution with heating time. It is also showed that graphene grown on Cu surfaces with varied orientations has totally different growth behaviors. The results would greatly facilitate the high-throughput determination of Cu surface index and accelerate the large-scale facet-dependent catalytic research of Cu, such as in single-crystal graphene growth.

Cu(111), Cu(100), and Cu(110), yielded distinct growth results.^[9–13] Recently, scientists have developed advanced annealing techniques to produce single-crystal Cu from industrial Cu foils,^[10] although the accurate control of the surface type is still of great challenge. To fully utilize the surface-dependent activity and functionality of Cu foil for future industrial-level applications, it is a prerequisite to accurately identify the Cu surface index in large scale. To date, the prevailing methods to determine Cu surface type are mainly based on high-vacuum surface techniques, such as scanning tunneling microscope, low-energy electron diffraction (LEED), and electron backscatter diffraction.^[4–14] Unfortunately, these techniques are all of low throughput and in small scale ranging from nanometers to millimeters. Therefore, there is an urgent demand to develop a convenient method to obtain the surface

Copper (Cu) has been widely used as a catalytic substrate to grow 2D materials, such as graphene and hexagonal boron nitride (h-BN).^[1–11] Especially since the first successful graphene growth on Cu, numerous efforts have been made to the mass production of high-quality graphene films on single-crystal Cu.^[9,10] It was found that different Cu surfaces, for example

index of Cu in large scale with high throughput.


In this work, we demonstrate an optical contrast method to determine the Cu surface type in scale up to meter size. After mildly oxidizing the Cu in hot air between 100 and 250 °C for a certain time (less than 3 h), different Cu surfaces show distinct colors. Detailed analysis and numerical simulations reveal that the color difference originates from the Cu₂O thickness difference (the multireflection between air/Cu₂O and Cu₂O/Cu interfaces leads to different colors), which is determined by the surface-index-dependent oxidation barriers of Cu. The barrier values of three typical surface of (111), (100), and (110) are further extracted from the color evolution under different temperatures. Our method enables the high-throughput determination of Cu surface index and will likely accelerate the large-scale facet-dependent catalytic research of Cu, such as in the single-crystal graphene and h-BN growth.

It is known that Cu foils can be gradually oxidized in air with mainly Cu₂O on its surface (Figure 1a). This natural oxidation of Cu in air is pretty slow and the formation of Cu₂O will further slowdown the oxidation.^[15] To accelerate the oxidation process, we typically heat the Cu foil in hot air (100–250 °C) by oven. The formation of Cu₂O on Cu surface can be readily verified by Raman spectroscopy and atomic force microscopy (AFM). We partially cover the Cu surface with chemical vapor deposition (CVD) grown graphene domains.^[1] Utilizing the antioxidation capacity of graphene, graphene-coated Cu will keep unoxidized but the bare Cu gets oxidized in hot air (at 200 °C for 5 min).^[16,17] The Raman spectra on

Z. B. Zhang, X. Z. Xu, Z. H. Zhang, M. H. Wu, J. H. Wang,
C. Liu, N. Z. Shang, J. X. Wang, Prof. K. H. Liu
State Key Laboratory for Mesoscopic Physics
School of Physics
Peking University
Beijing 100871, China
E-mail: khliu@pku.edu.cn

Z. H. Zhang, C. Liu, N. Z. Shang
Academy for Advanced Interdisciplinary Studies
Peking University
Beijing 100871, China
Prof. P. Gao, Prof. E. G. Wang
International Centre for Quantum Materials
Peking University
Beijing 100871, China

Prof. D. P. Yu
Department of Physics
South University of Science and Technology of China
Shenzhen 518055, China

 The ORCID identification number(s) for the author(s) of this article can be found under <https://doi.org/10.1002/admi.201800377>.

DOI: 10.1002/admi.201800377

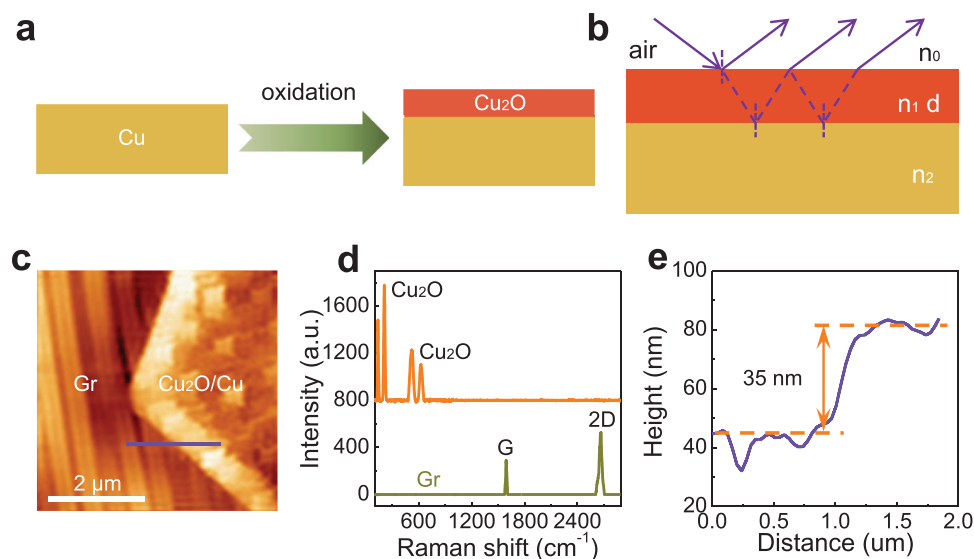


Figure 1. Oxidation of Cu surface. a) Schematic diagram of Cu oxidation process under mild circumstance. b) Schematic diagram of multireflection of $\text{Cu}_2\text{O}/\text{Cu}$; n_0 , n_1 , and n_2 represent the refractive index of air, Cu_2O , and Cu, respectively; d refers to the thickness of Cu_2O layer. c) Atomic force microscopic image of a Cu surface partially coated with graphene. The scale bar is 2 μm . d) Raman spectra of graphene-coated and bare Cu area, indicating that the oxidation products are mainly Cu_2O . e) The height profile along the purple line in (c).

graphene/Cu show only graphene signal, while on bare Cu region characteristic Cu_2O peaks come up (Figure 1d).^[17] Further AFM characterization reveals that the $\text{Cu}_2\text{O}/\text{Cu}$ region is higher than the graphene/Cu region by about 35 nm (Figure 1c,e), which is due to the smaller mass density of Cu_2O to Cu. Previous results show that under severe oxidation at higher temperature, CuO might be further formed on the top of Cu_2O layer, but in our mild oxidation condition, no CuO signal can be detected.^[18,19]

Once the Cu_2O layer is formed on Cu surface, the multireflection between air/ Cu_2O and $\text{Cu}_2\text{O}/\text{Cu}$ interfaces will lead to a specific color under white light illumination (Figure 1b). The optical contrast ($C(\lambda) = 1 - \frac{R_1(\lambda)}{R_0(\lambda)}$), where R_0 is the reflected light intensity from the bare Cu, and R_1 is that from the $\text{Cu}_2\text{O}/\text{Cu}$ can be obtained by the solution of Snell's equation.^[20–24] The only variant is the thickness of Cu_2O (d), and different d gives out different colors.

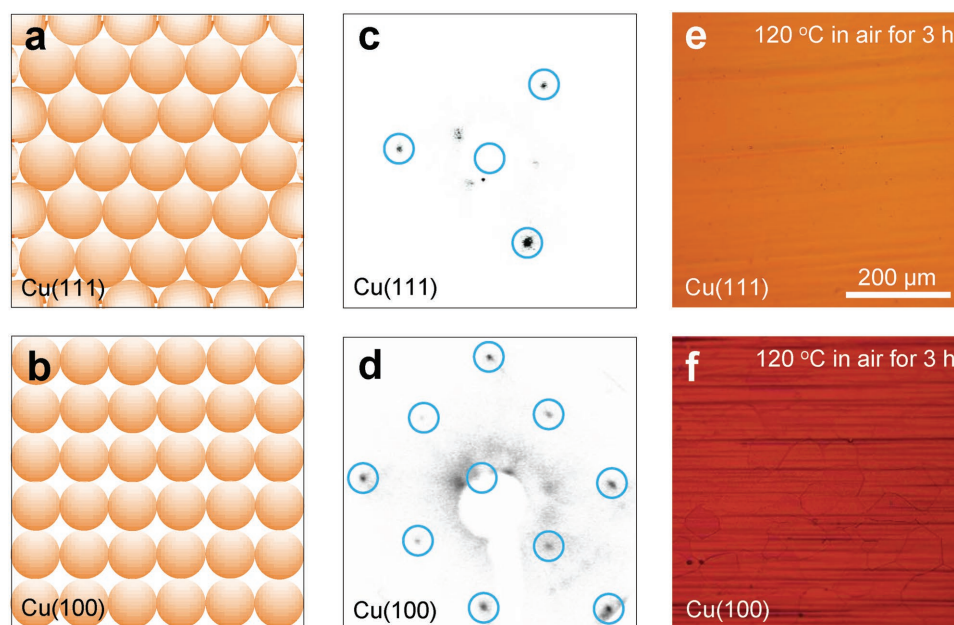


Figure 2. Surface-dependent color of oxidized Cu(111) and Cu(100) surfaces. a,b) Schematic diagrams of the atomic lattice for Cu(111) and Cu(100). c,d) The low energy electron diffraction patterns of Cu(111) and Cu(100). e,f) Optical images of Cu(111) and Cu(100) after heating in air at 120 °C for 3 h. The image size of (e) and (f) is same.

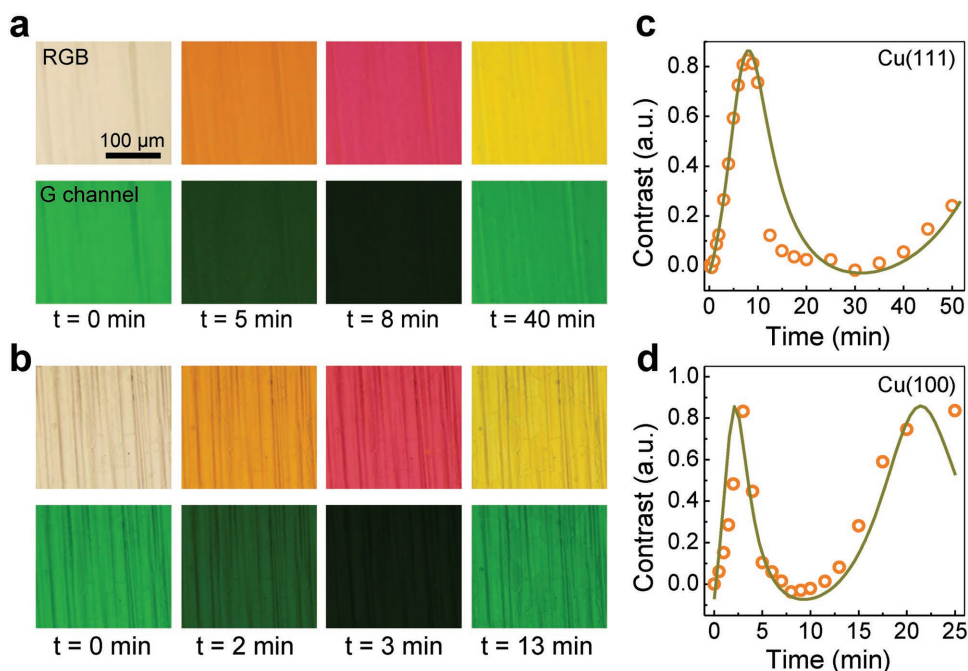


Figure 3. Optical contrast evolution of Cu(111) and Cu(100) surfaces under oxidation. a,b) Optical images of Cu(111) and Cu(100) after heating at 200 °C for different time. The first row is taken under natural light and the second row are the images filtered by a 550 nm bandpass filter. There is no light polarization setting in the characterization. The image size is same for all the images. c,d) Plot and fit of the optical contrast for Cu(111) and Cu(100) as a function of oxidation time at 200 °C.

In our experiment, we choose three prevailing surfaces in the growth of graphene, Cu(111), Cu(100), and Cu(110) (Figure 2; Figure S1, Supporting Information), for demonstration. The atomic models and LEED patterns for Cu(111) and Cu(100) surfaces are shown in Figure 2a–d. After oxidation under the same condition (at 120 °C for 3 h), the colors of Cu(111) and Cu(100) both change dramatically but are quite distinct with each other (Figure 2e,f). This result reveals that it is realistic to employ the optical color to distinguish different type of Cu surfaces.

To have a more quantitative understanding of the relation between color and surface type, we investigate the in situ color evolution of two Cu foils (Cu(111) and Cu(100)) at different oxidation time in air at 200 °C (Figure 3a,b). We directly recorded the colorful images as well as filtered images ($\lambda = 540 \pm 10$ nm) with natural light for quantitative analysis. As the oxidation time lapses, the colorful images firstly turn to red and then convert back to yellow (the first row in Figure 3a,b), while filtered images first turn to dark and then bright again (the second row in Figure 3a,b). This behavior can be understood quantitatively by describing the oxide thickness (d) as a function of time (t), where d can be expressed as

$$d = kt^{1/2} + d_0 \quad (1)$$

in which k describes the oxidization rate and d_0 is a constant.^[25,26]

By using the double-layer model (Cu₂O/Cu), the experiment data obtained can be well fitted (Figure 3c,d) and thus the oxidation rate (k) can be acquired from the fitting. The k for Cu(100) is 32 ± 2 nm min^{-1/2}, much faster than that of Cu(111)

(19 ± 1 nm min^{-1/2}), which means to form the same thickness of Cu₂O, Cu(111) needs much more time.

According to the Arrhenius equation

$$k = Ae^{-E/k_bT} \quad (2)$$

where A is a constant, E is the oxidation barrier, k_b is the Boltzmann constant, and T is absolute temperature, the oxidation rate difference for different Cu surfaces is originating from the barrier difference.^[4] Qualitatively, higher oxidation barrier results in slower oxidation rate. To obtain the oxidation barriers of different Cu surfaces, we perform series in situ color evolution experiments and get corresponding oxidation rates (k) at different temperatures (Figure 4a,d). Combining with the Arrhenius equation, we plot the growth rate as a function of temperature (Figure 4e,f), in which the slope obtained by “least square fitting” method is corresponding to the oxidation barrier for each surface. The results are $E = 0.24$ eV for Cu(111), $E = 0.22$ eV for Cu(100) and $E = 0.12$ eV for Cu(110) (Figure S2, Supporting Information). As different surface types have different E , the color evolution can be therefore used to determine the surface index unambiguously. Our method is based on optical contrast and therefore naturally enables high-throughput determination of Cu surface index for large Cu foils readily up to meter scale. Further control experiments also show that this technique is of wide applicability for Cu foils from different suppliers (Figures S3 and S4, Supporting Information).

Identifying the Cu surface index quickly in large area is very important to the catalytic growth of 2D materials. Here we use graphene grown on Cu(111) and Cu(100) as an example,

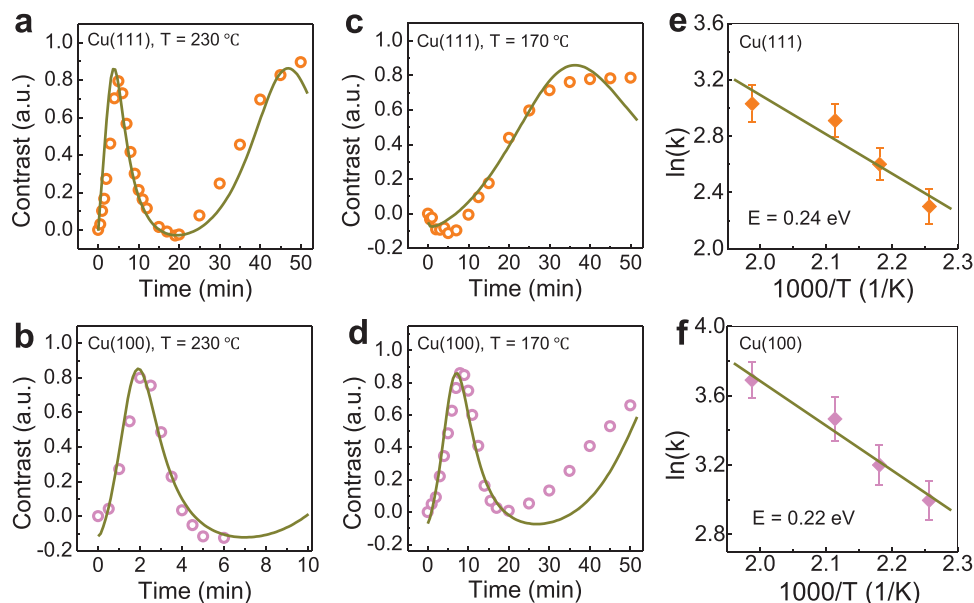


Figure 4. Oxidation barriers of Cu(111) and Cu(100). a–d) Plot and fit of the optical contrast for Cu(111) and Cu(100) as a function of oxidation time at 230 and 170 °C. e, f) Plot and fit of the oxidation rate for Cu(111) and Cu(100) as a function of temperature. The oxidation barrier obtained are $E = 0.24$ and 0.22 eV for Cu(111) and Cu(100), respectively.

showing that there is a strong correlation between the property (such as morphology, crystallographic orientation, and doping effect) of graphene and the surface index of underlying Cu substrate. Visually, optical images of graphene domains exhibit the shape of hexagonal on Cu(111) while quadrilateral on Cu(100). We also notice that on both substrates all graphene domains are aligned (Figure 5a,b), which is consistent with previous reports.^[9,10] However, further LEED characterizations

reveal that the graphene domains on Cu(111) indeed have the same crystallographic orientation (Figure 5c); while graphene domains on Cu(100) do not (Figure 5d). That is because graphene lattice (C_6 rotation symmetry) can grow epitaxially on Cu(111) (C_3 rotation symmetry) but not on Cu(100) (C_4 rotation symmetry), so the deceptive alignment of quadrilateral graphene domains on Cu(100) may originate from the modulation of substrate's fourfold symmetry (Figure 5b).

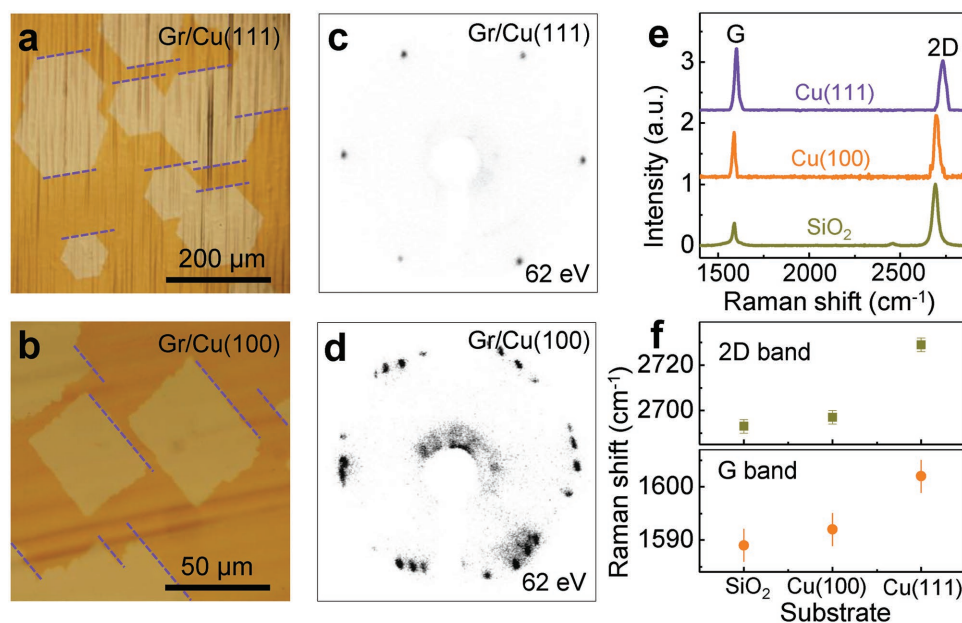


Figure 5. Graphene grown on Cu(111) and Cu(100). a, b) Optical images of graphene domains on Cu(111) and Cu(100). Domains are hexagonal on Cu(111) and quadrilateral on Cu(100). Graphene domains on both Cu(111) and Cu(100) are aligned. c, d) LEED patterns of graphene on Cu(111) and Cu(100). Crystallographic direction of graphene on Cu(111) is same but randomly on Cu(100). e) Raman spectra of graphene on Cu(111), Cu(100), and SiO_2 substrate. f) Peak positions of 2D band and G band of graphene on Cu(111), Cu(100), and SiO_2 substrate.

Further Raman measurements were carried out to testify the charge transfer of graphene/Cu(111) and Cu(100). The Raman spectrum of graphene on Cu(111) shows that the G peak is strongly blue shifted and the intensity ratio of 2D/G decreases obviously due to the strong doping effect (Figure 5e,f).^[27,28] As a contrast, Raman spectrum of graphene on Cu(100) changes little compared with graphene transferred onto SiO₂/Si substrate. Quantitatively analysis gives out a $\approx 2.0 \times 10^{13} \text{ cm}^{-2}$ and $\approx 0.5 \times 10^{13} \text{ cm}^{-2}$ hole doping concentrations of graphene on Cu(111) and Cu(100), respectively.^[27,28] This different doping level of graphene on Cu(111) and Cu(100) can be understood considering that graphene/Cu(111) is a commensurate system with strong interfacial coupling and charge transfer effect, while graphene/Cu(100) is an incommensurate system with weaker interfacial coupling.^[17]

In summary, our work presents a high-throughput and easily performed characterization technique in the identification of Cu surface index, and it can be further generalized to other metals. Also, the oxidation barrier of Cu surface can be quantitatively obtained from the color evolution during heating. Our method paves a new direction of the high-throughput determination of Cu surface index and will accelerate the large-scale facet-dependent 2D materials growth on Cu, such as single-crystal graphene and h-BN.

Experimental Section

Growth of Partially Coated Graphene Samples: Graphene samples were grown by CVD method using CH₄ as precursors. The CVD process was performed under ambient pressure with ultrahigh-purity argon gas. The process is to heat Cu from room temperature to 1010 °C with 500 sccm Ar for 75 min, keep at 1010 °C with 50 sccm H₂ for 40 min, grow graphene with 10 sccm H₂ and 0.5 sccm CH₄ for 1 h, and then naturally cool down to room temperature.

Characterization: Raman spectroscopy was taken by a LabRAM HR800 system with laser excitation wavelength of 633 nm. The Cu fluorescent background is removed to make characteristic peaks clearer. Optical images were taken by an Olympus microscope (Olympus BX53M).

Supporting Information

Supporting Information is available from the Wiley Online Library or from the author.

Acknowledgements

Z.B.Z. and X.Z.X. contributed equally to this work. This work was supported by the National Key R&D Program of China (2016YFA0300903 and 2016YFA0200103), the NSFC (51522201 and 11474006), the National Equipment Program of China (ZDY2015-1), Beijing Graphene Innovation Program (Z161100002116028), National Postdoctoral Program for Innovative Talents (BX201700014), and the National Program for Thousand Young Talents of China.

Conflict of Interest

The authors declare no conflict of interest.

Keywords

graphene, optical contrast, oxidation barrier, surface index

Received: March 6, 2018

Revised: April 11, 2018

Published online: May 16, 2018

- [1] X. S. Li, W. W. Cai, J. H. An, S. Kim, J. Nah, D. X. Yang, R. Piner, A. Velamakanni, I. Jung, E. Tutuc, S. K. Banerjee, L. Colombo, R. S. Ruoff, *Science* **2009**, 324, 1312.
- [2] L. X. Liu, H. L. Zhou, R. Cheng, W. J. Yu, Y. Liu, Y. Chen, J. Shaw, X. Zhong, Y. Huang, X. F. Duan, *ACS Nano* **2012**, 6, 8241.
- [3] K. K. Kim, A. Hsu, X. T. Jia, S. M. Kim, Y. S. Shi, M. Hofmann, D. Nezich, J. F. Rodriguez-Nieva, M. Dresselhaus, T. Palacios, J. Kong, *Nano Lett.* **2012**, 12, 161.
- [4] Y. F. Hao, M. S. Bharathi, L. Wang, Y. Y. Liu, H. Chen, S. Nie, X. H. Wang, H. Chou, C. Tan, B. Fallahzad, H. Ramanarayan, C. W. Magnuson, E. Tutuc, B. I. Yakobson, K. F. McCarty, Y. W. Zhang, P. Kim, J. Hone, L. Colombo, R. S. Ruoff, *Science* **2013**, 342, 720.
- [5] L. Liu, J. Park, D. A. Siegel, K. F. McCarty, K. W. Clark, W. Deng, L. Basile, J. C. Idrobo, A. P. Li, G. Gu, *Science* **2014**, 343, 163.
- [6] X. J. Song, J. F. Gao, Y. F. Nie, T. Gao, J. Y. Sun, D. L. Ma, Q. C. Li, Y. B. Chen, C. H. Jin, A. Bachmatiuk, M. H. Ruemmel, F. Ding, Y. F. Zhang, Z. F. Liu, *Nano Res.* **2015**, 8, 3164.
- [7] R. Y. Tay, H. J. Park, G. H. Ryu, D. L. Tan, S. H. Tsang, H. L. Li, W. W. Liu, E. H. T. Teo, Z. Lee, Y. Lifshitz, R. S. Ruoff, *Nanoscale* **2016**, 8, 2434.
- [8] X. Z. Xu, Z. H. Zhang, L. Qiu, J. N. Zhuang, L. Zhang, H. Wang, C. N. Liao, H. D. Song, R. X. Qiao, P. Gao, Z. H. Hu, L. Liao, Z. M. Liao, D. P. Yu, E. G. Wang, F. Ding, H. L. Peng, K. H. Liu, *Nat. Nanotechnol.* **2016**, 11, 930.
- [9] H. Wang, X. Z. Xu, J. Y. Li, L. Lin, L. Z. Sun, X. Sun, S. L. Zhao, C. W. Tan, C. Chen, W. H. Dang, H. Y. Ren, J. C. Zhang, B. Deng, A. L. Koh, L. Liao, N. Kang, Y. L. Chen, H. Q. Xu, F. Ding, K. H. Liu, H. L. Peng, Z. F. Liu, *Adv. Mater.* **2016**, 28, 8968.
- [10] X. Z. Xu, Z. H. Zhang, J. C. Dong, D. Yi, J. J. Niu, M. H. Wu, L. Lin, R. K. Yin, M. Q. Li, J. Y. Zhou, S. X. Wang, J. L. Sun, X. J. Duan, P. Gao, Y. Jiang, X. S. Wu, H. L. Peng, R. S. Ruoff, Z. F. Liu, D. P. Yu, E. G. Wang, F. Ding, K. H. Liu, *Sci. Bull.* **2017**, 62, 1074.
- [11] Z. H. Zhang, X. Z. Xu, L. Qiu, S. X. Wang, T. W. Wu, F. Ding, H. L. Peng, K. H. Liu, *Adv. Sci.* **2017**, 4, 1700087.
- [12] Y. Ogawa, B. S. Hu, C. M. Orofeo, M. Tsuji, K. Ikeda, S. Mizuno, H. Hibino, H. Ago, *J. Phys. Chem. Lett.* **2012**, 3, 219.
- [13] A. T. Murdock, A. Koos, T. Ben Britton, L. Houben, T. Batten, T. Zhang, A. J. Wilkinson, R. E. Dunin-Borkowski, C. E. Lekka, N. Grobert, *ACS Nano* **2013**, 7, 1351.
- [14] L. Meng, Y. L. Wang, L. Z. Zhang, S. X. Du, R. T. Wu, L. F. Li, Y. Zhang, G. Li, H. T. Zhou, W. A. Hofer, H. J. Gao, *Nano Lett.* **2013**, 13, 685.
- [15] J. C. Yang, B. Kolasa, J. M. Gibson, M. Yeadon, *Appl. Phys. Lett.* **1998**, 73, 2841.
- [16] S. S. Chen, L. Brown, M. Levendorf, W. W. Cai, S. Y. Ju, J. Edgeworth, X. S. Li, C. W. Magnuson, A. Velamakanni, R. D. Piner, J. Y. Kang, J. Park, R. S. Ruoff, *ACS Nano* **2011**, 5, 1321.
- [17] X. Z. Xu, D. Yi, Z. C. Wang, J. C. Yu, Z. H. Zhang, R. X. Qiao, Z. H. Sun, Z. H. Hu, P. Gao, H. L. Peng, Z. F. Liu, D. P. Yu, E. G. Wang, Y. Jiang, F. Ding, K. H. Liu, *Adv. Mater.* **2018**, 30, 1702944.
- [18] J. Gao, A. M. Hu, M. Li, D. L. Mao, *Appl. Surf. Sci.* **2009**, 255, 5943.
- [19] Y. Tomioka, J. Miyake, *IEEE Proc. of 49th Electronic Components & Technology Conf.*, IEEE, San Diego, CA **1999**, p. 714.
- [20] L. B. Gao, W. C. Ren, F. Li, H. M. Cheng, *ACS Nano* **2008**, 2, 1625.

- [21] H. Li, J. M. T. Wu, X. Huang, G. Lu, J. Yang, X. Lu, Q. H. Zhang, H. Zhang, *ACS Nano* **2013**, 7, 10344.
- [22] X. L. Li, W. P. Han, J. B. Wu, X. F. Qiao, J. Zhang, P. H. Tan, *Adv. Funct. Mater.* **2017**, 27, 1604468.
- [23] Z. H. Ni, H. M. Wang, J. Kasim, H. M. Fan, T. Yu, Y. H. Wu, Y. P. Feng, Z. X. Shen, *Nano Lett* **2007**, 7, 2758.
- [24] Y. Y. Wang, R. X. Gao, Z. H. Ni, H. He, S. P. Guo, H. P. Yang, C. X. Cong, T. Yu, *Nanotechnology* **2012**, 23, 495713.
- [25] I. C. Cheng, A. M. Hodge, *Adv. Eng. Mater.* **2012**, 14, 219.
- [26] K. F. Chen, S. Y. Song, D. F. Xue, *CrystEngComm* **2013**, 15, 144.
- [27] A. Das, S. Pisana, B. Chakraborty, S. Piscanec, S. K. Saha, U. V. Waghmare, K. S. Novoselov, H. R. Krishnamurthy, A. K. Geim, A. C. Ferrari, A. K. Sood, *Nat. Nanotechnol.* **2008**, 3, 210.
- [28] J. Yan, Y. B. Zhang, P. Kim, A. Pinczuk, *Phys. Rev. Lett.* **2007**, 98, 166802.